Bulletin of Mathematical Biology Vol. 55, No. 1, pp. 155–174, 1993.
Printed in Great Britain.

0092–8240/93$5.00+0.00
Pergamon Press Ltd

THEORETICAL STUDY OF THE OPTIMAL SHAPE OF THE FRONT PROFILE OF THE LENS IN THE EYE OF THE SCALLOP, *PECTEN*

■ GÁBOR HORVÁTH
Central Research Institute for Physics,
Hungarian Academy of Sciences,
Biophysics Group, H-1525 Budapest,
P.O.B. 49, Hungary

■ DEZSÖ VARJÚ
Universität Tübingen,
Lehrstuhl für Biokybernetik,
Auf der Morgenstelle 28,
D-7400 Tübingen 1,
Germany

The optimal shape of the front profile of the thick lens in the eye of the scallop, *Pecten* is theoretically, geometric optically investigated as a function of the refractive index of the lens and the retina, as well as of the geometrical parameters of the eye. The shape of the theoretical front surfaces is compared with that of the real, experimentally determined front face of the lens. The degree of correction of the lens for spherical aberration of the reflecting spherical mirror in the *Pecten* eye is examined. The optimal shape of the front profile of the lens depends strongly on a set of parameters, such that a certain fine tuning is required among them to assure a full correction for spherical aberration. The extreme variability of the eye parameters and the shape of the front face of the lens in the scallop is inconsistent with this fine tuning requirement. The degree of correction of the *Pecten* lens for spherical aberration might not be as good as it could be, a possible biooptical reason for which is discussed.

1. Introduction. After a series of histological investigations of the eye of the scallop, *Pecten* (Patten, 1886; Dakin, 1910), Land (1965, 1966a,b, 1968) profoundly examined the optics of the eye in *Pecten*, and assessed the nature and quality of the visual image produced. The eye of *Pecten* possesses an unusual optical system (Fig. 1). The back of the eye is lined with an accurately spherical, highly reflecting layer called *argentea* (or *tapetum lucidum*); the eye is a combination of a concave mirror and a thick lens with a bell-shaped front surface. The *argentea* is not a reflector designed to increase sensitivity at low light intensities, as in the eyes of some mammals and fishes (Denton, 1970, 1971), where the visual image is formed by a lens only. In the *Pecten* eye the lens alone would form an image far behind the retina. The lens has the function of correcting for the spherical aberration of the *argentea* by means of a special

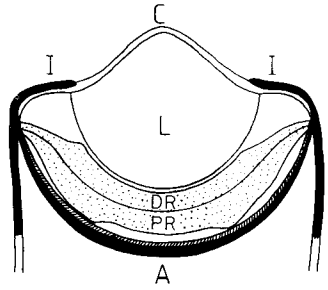

Figure 1. Schematic diagram of the median section of the *Pecten* eye (Land, 1965). C: cornea, I: iris, L: lens, DR: distal retina (dotted), PR: proximal retina (dotted), A: reflecting *argentea* or *tapetum lucidum* (hatched).

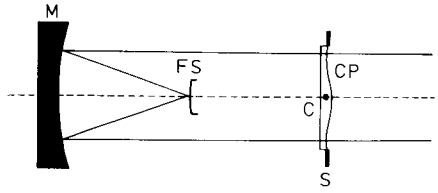

Figure 2. The structure of the Schmidt astronomical telescope. M: spherical mirror, FS: focal surface, S: stop, CP: corrector plate, C: centre of curvature of the mirror (Born and Wolf, 1964).

bell-shaped front face, as the corrector plates in the different types of the Schmidt astronomical telescopes (Fig. 2) (Born and Wolf, 1964).

On the basis of responses recorded in the distal and proximal retinae to different stimuli (Hartline, 1938; Kennedy, 1963; Land, 1966a, 1968) and from ethological observations (Buddenbrock and Moller-Racke, 1953; Land, 1965, 1968) it could be deduced that two aspects of the visual environment are important to scallops: the overall level of illumination, and its small local or total changes caused by shadows or image movements. Information relating to these two aspects is extracted by two separate receptor systems in the retina (Fig. 1).

Such highly optimized optical systems appear to be rather rare in the animal kingdom. Except in scallops, they have been described only in certain extinct fossil trilobites (Clarkson and Levi-Setti, 1975) and in the water bug backswimmer (Schwind, 1980).

Trilobites with schizochroal eyes (phacopid trilobites, for example) and the backswimmer (*Notonecta glauca*) have thick corneal lenses with two optically different but homogeneous units, separated by a special fourth-degree interface

which corrects for spherical aberration. Trilobites needed these lenses to increase the light-collecting efficiency and transfer of contrast, as does the backswimmer.

The geometrical optics of the trilobite and *Notonecta* eyes and the maturation of trilobite vision are profoundly investigated; the theoretical shapes of the separating interfaces in their corneal lenses depending on different optical and geometrical parameters of the eye have been determined; the theoretically calculated surfaces agree almost exactly with those found in the eyes (Horváth, 1989a,b; Horváth and Greguss, 1989a,b; Horváth and Clarkson, 1992).

The optics of the *Pecten* eye is thoroughly examined experimentally (Land, 1965, 1966b); however, geometric optical investigations comparing the optimal theoretical shape of the front surface with that of the real one in *Pecten* have not yet been carried out. The results accumulated in investigating different types of the Schmidt telescope (Fig. 2) are only of limited value in this respect, since their structure and the relative dimension of their parts differ significantly from those of the *Pecten* eye. For example, the relative aperture (or focal ratio) A = focal length/absolute aperture of these equipments is not lower than about three (Born and Wolf, 1964), whilst in the *Pecten* eye it amounts to $A = 0.6$ (Land, 1965).

The aim of this work is to determine theoretically the shape of the optimal front surface of the scallop lens as a function of the refractive indices and the geometrical parameters of the eye. Comparing such theoretical profiles to the real ones, one can estimate to what degree the spherical aberration of the *Pecten* lens is corrected for.

2. The Eye and Behaviour of the Scallop. The scallop *Pecten* has a large number of pallial eyes, about 60 in *Pecten maximus*, for example, the diameter of which amounts to 0.9–1 mm. A real image is formed in the eye by the refraction through a thick lens and by the reflection at the *argentea* (Fig. 1), a multilayer structure composed of guanin crystals which functions as a highly efficient reflector for blue–green light. The *argentea* lines the whole of the back of the eye, and it is spherical, or very nearly so. This layer gives the pupil of the eye its blue–green bright iridescent appearance (Land, 1966b).

The image falls on the region of the retina occupied by the ciliary lamellae of the distal cells. The optical function of the thick lens is to provide a certain amount of correction for the spherical aberration, an inherent property of the spherical *argentea* (Land, 1965).

The refractive index of the lens is uniform, $n_L = 1.42$, and unlike the lenses of the eyes of fishes, the lens of *Pecten* is soft throughout; there is no hard protein core and soft periphery, as in the fish lens. Observations on the isolated retina and on individual cells indicate that only the outer segments, a layer less than

40 μm thick, have a refractive index substantially higher than sea water ($n_w = 1.34$).

The shape of the lens was determined by means of photographs of frozen sections (Land, 1965). The rear surface of the lens is spherical, the front face is bell-shaped, but its profile varies considerably.

The retina occupies the space between the lens and the *argentea* (Fig. 1). It consists of two main cell layers. Since the proximal retina is very close to the *argentea* (10–40 μm in the centre of the eye), no image is formed on it. Between the proximal retina and the lens is a second layer of cells, the distal retina, where the image is formed. There are approximately 5 000 receptors in each retinae in *Pecten maximus*, for example, and each gives rise to a fibre in the optic nerve (Land, 1968).

Cells of the distal retina respond to the decrease (OFF-cells) and cells of the proximal retina to the increase (ON-cells) of the level of illumination (Hartline, 1938; Land, 1966a). The ON-cells also continue to respond during prolonged illumination. Thus, the OFF-cells of the distal retina respond to the trailing edges of light objects, and to the leading edges of dark ones. The OFF-system is highly directionally selective and is, therefore, involved in movement perception. The primary function of the ON-cells in the proximal retina, where no image is formed, is to monitor the level of illumination.

The eye of *Pecten* collects light very efficiently. The visual field of each eye extends to 90–110° (Land, 1965; Buddenbrock and Moller-Racke, 1953). The extremely small focal ratio $A = 0.6$ provides an aperture wider than that of any known eye which forms an image through a lens. The best among them, the eyes of fish, have a focal ratio $A = 0.8$. The *Pecten* mirror with such a large aperture, however, has great spherical aberration, and therefore poor resolution. But if the profile of the lens corresponded exactly to the theoretical profile of a Schmidt system (Fig. 2) without spherical aberration, then the angular resolution in the axial part of the image could approach the minimum value given by $d = 1.2\lambda/D$, where λ is the wave length of the incident light, and D is the diameter of the pupil. Since the diameter d of the Airy diffraction disk (circle of confusion) on the retina would be less than 1 μm, the visual resolution of the *Pecten* eye would be limited in this case not by the quality of the image, but by the density of the cells in the distal retina; their distance is about 5 μm in the centre, and 10 μm towards the edges (Land, 1965, 1968).

The most relevant stimuli to which the scallops respond are: (i) the distribution of brightness in the surround; (ii) reduction of light intensity by shadowing; (iii) movements of objects in the optical environment. These stimuli result in different patterns of behaviour (Buddenbrock and Moller-Racke, 1953). Stimulus (i) controls the direction in which the animals swim, and prior to this the direction in which the tentacles are extended. The receptors mediating these responses are the cells of the proximal retina;

information about stationary patterns of illumination is only available from these receptors.

All *Pecten* species respond in much the same way to stimuli (ii) and (iii) by withdrawing the tentacles and closing the valves. The most sensitive species, *Pecten irradians*, responds to a 5.4% decrease of the overall illumination, and to a 0.52% decrease, when it is caused by a moving object. Dark objects cause closure of *Pecten varius* if they move through 1° relative to the animal (Buddenbrock and Moller-Racke, 1953). Such excellent sensitivity to shadowing and object movement is made possible by the relative good quality image formed on the distal retina (Land, 1968).

3. Calculation of the Front Profile of the *Pecten* Lens. Consider the system of coordinates of Fig. 3, which represents half of a median section through the *Pecten* eye. The vertical axis coincides with the optical axis of the eye. The section of the front and rear surface of the lens, and that of the reflecting *argentea* are described by the functions $e(x)$, $L(y)$ and $m(z)$, respectively. The axial thickness of the lens is a, the axial distance between the rear surface of the lens and the *argentea* is b, the radius of the cylindrical eye is r. The refractive indices of the sea water, the optically homogeneous lens and retina are n_w, n_L and n_r, respectively.

Figure 3 shows the path of a paraxial ray of incident light in the eye, which intersects the optical axis in the focal point F at distance f from the *argentea*. We calculate that curve $e(x)$, which assures that all the paraxial rays of light at any radial distance intersect the optical axis at the same focal point F after refraction on the front and rear surface of the lens and after reflexion on the *argentea*. This means that the eye is corrected for spherical aberration, that is, it has an exact focal point F.

Referring to Fig. 3, and using the refraction law of Snellius and DesCartes, we obtain the relationship:

$$\frac{\sin \alpha}{\sin \beta} = \frac{n_L}{n_w} \tag{1}$$

$$\frac{\sin \gamma}{\sin \delta} = \frac{n_r}{n_L} \tag{2}$$

and furthermore

$$\tan \alpha = -e'(x) \equiv -\mathrm{d}e/\mathrm{d}x \tag{3}$$

$$\tan \varepsilon = L'(y) \equiv \mathrm{d}L/\mathrm{d}y \tag{4}$$

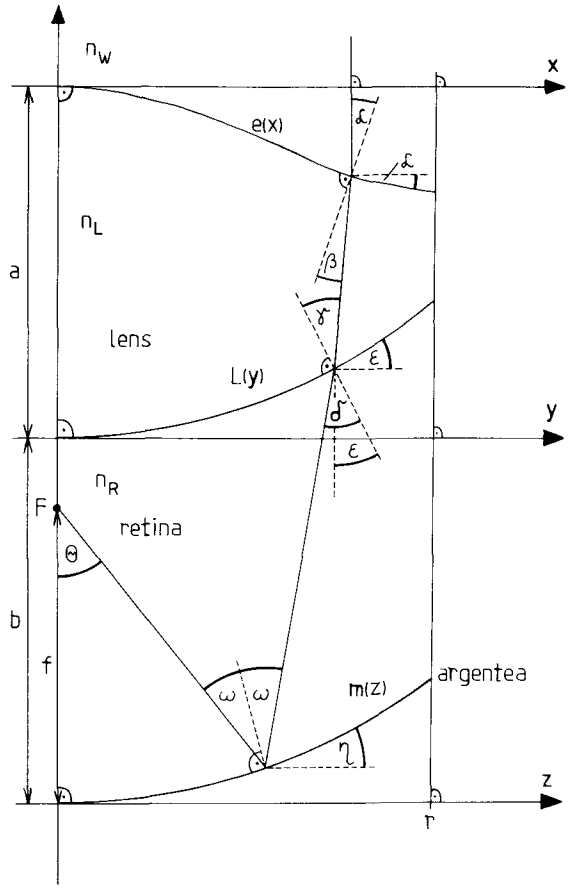

Figure 3. Half of the median section of the model *Pecten* eye containing its optical axis, and the path of a paraxial incident ray of light in the eye.

$$\tan \eta = m'(z) \equiv \mathrm{d}m/\mathrm{d}z \tag{5}$$

$$\gamma + \beta = \alpha + \varepsilon \tag{6}$$

$$\omega + \varepsilon = \delta + \eta \tag{7}$$

$$\theta + \delta = 2\omega + \varepsilon \tag{8}$$

$$x = y + [a + e(x) - L(y)]\tan(\alpha - \beta) \tag{9}$$

$$y = z + [b + L(y) - m(z)]\tan(\delta - \varepsilon) \tag{10}$$

$$z=[f-m(z)]\tan\theta. \tag{11}$$

From (5), (7), (8), (10) and (11) we derive:

$$H(y)\equiv z-y+[b+L(y)-m(z)]S(z)=0$$
$$S(z)\equiv\tan(\delta-\varepsilon)=\frac{z[1-m'(z)^2]-2m'(z)[f-m(z)]}{2zm'(z)+[f-m(z)]\,[1-m'(z)^2]}. \tag{12}$$

From (2), (4–9) and (11):

$$x=y+[a+e(x)-L(y)]T \tag{13}$$

follows, where:

$$T\equiv\tan(\alpha-\beta)=\tan\left[\arcsin\left(\frac{n_r}{n_L}\sin D\right)-\arctan L'(y)\right] \tag{14}$$

with:

$$D\equiv\delta=\arctan L'(y)+\arctan\left[\frac{z}{f-m(z)}\right]-2\arctan m'(z). \tag{15}$$

From (3):

$$-\tan\alpha_{i-1}\equiv -t_{i-1}=e'(x_{i-1})=\frac{e_i-e_{i-1}}{x_i-x_{i-1}} \tag{16}$$

can be derived. From (13) and (16) we obtain:

$$e_i=\frac{e_{i-1}+t_{i-1}[y_{i-1}-y_i+a(T_{i-1}-T_i)+T_{i-1}e_{i-1}+T_iL(y_i)-T_{i-1}L(y_{i-1})]}{1+T_it_{i-1}}, \tag{17}$$

and from (1) and (14):

$$G(t)\equiv\sum_{n=0}^{4}g_nt^n=0,\quad t\equiv\tan\alpha,\quad g_0=T^2n_L^2,\quad g_1=-2Tn_L^2,$$
$$g_2=(n_L^2-n_w^2)(1+T^2),\quad g_3=g_1,\quad g_4=n_L^2-n_w^2(1+T^2). \tag{18}$$

Having these relationships the function $e(x)$ can be derived in the following way. For a given series $[z_i=i\Delta z;\ \Delta z=r/m;\ 1\ll m\in N;\ i=1, 2, \ldots, m]$ the set $[y_i]$ can be determined from (12), then the series $[D_i]$ from (15), the set $[T_i]$ from (14), the series $[t_i]$ from (18). Equations (12) and (18) can be solved for y and t numerically. We used the tangent method of Newton, that is the recursions:

$$y_{k+1} = y_k - \frac{H(y_k)}{H'(y_k)}, \quad H'(y) \equiv \frac{dH}{dy} \tag{19}$$

$$t_{k+1} = t_k - \frac{G(t_k)}{G'(t_k)}, \quad G'(t) \equiv \frac{dG}{dt} \tag{20}$$

to calculate the approximate roots y_k and t_k. The algorithm to determine the series $[z_i]$, $[y_i]$, $[D_i]$, $[T_i]$ and $[t_i]$, mentioned above is illustrated schematically in Fig. 4A. Using the series $[y_i]$, $[T_i]$, $[t_i]$, the initial condition $e'(x=0)=0$,

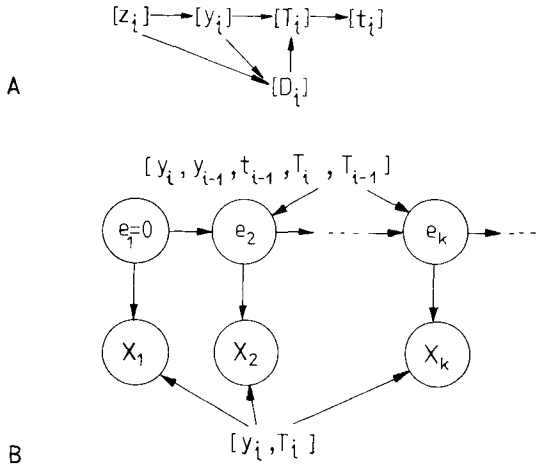

Figure 4. Schematic diagram of the algorithm to calculate the set $[t_i \equiv \tan \alpha_i]$ (A) and the series $[e_i, x_i]$ (B) for a given set $[z_i]$.

from which $e_1 = 0$ follows, and recursion (17), the set $[e_i]$ can be determined, then the series $[x_i]$ from (13). This algorithm is illustrated schematically in Fig. 4B. By means of these algorithms finally the set $[e_i, x_i]$ can be obtained for a given series of $[z_i]$.

On the basis of anatomical investigations the geometry of the *Pecten* eye can be described by the following spherical functions:

$$m(z) = R_t - (R_t^2 - z^2)^{1/2} \tag{21}$$

$$L(y) = R_L - (R_L^2 - y^2)^{1/2} \tag{22}$$

where R_t and R_L are the radii of curvature of the reflecting *argentea* and that of

the rear surface of the lens, respectively. The front surface of the lens can be well approximated by the fourth degree function:

$$c(\rho)=H\left(\frac{\rho}{\rho_H}\right)^4-2H\left(\frac{\rho}{\rho_H}\right)^2 \tag{23}$$

where $-H$ is the value of the absolute minimum at the abscissa ρ_H. The numerical value of the geometrical parameters a, b, R_t, R_L, H, ρ_H, r and the optical parameters n_L, n_r of two different typical *Pecten* eyes are given in Table 1. We refer to them as eye 1 and eye 2. Substituting (22) into (12), we obtain:

$$y(z)=\frac{J(z)}{1+S(z)^2}+\sigma\left\{\frac{J(z)^2}{[1+S(z)^2]^2}-\frac{J(z)^2-S(z)^2R_L^2}{1+S(z)^2}\right\}^{1/2}$$
$$J(z)=z+S(z)\,[b+R_L-m(z)]. \tag{24}$$

Table 1. Refractive indices of the *Pecten* eye and its surround, and numerical values (in μm) of the geometrical parameters of two different typical *Pecten* eyes. The numerical values of eye 1 and 2 originate from text-figure 8 and 1 of Land (1965), respectively

	n_w(Seawater)=1.34	n_L(Lens)=1.42	n_r(Retina)=1.34				
eye 1 (μm)	$a=380$	$b=165$	$R_t=390$	$R_L=235$	$H=155$	$\rho_H=240$	$r=210$
eye 2 (μm)	$a=410$	$b=140$	$R_t=390$	$R_L=250$	$H=150$	$\rho_H=250$	$r=230$

Referring to Fig. 5, the following condition can be derived for the parameter σ in (24):

$$\sigma=-1 \quad \text{if} \quad S(z)\equiv\tan(\delta-\varepsilon)\geqslant 0,$$
$$\sigma=+1 \quad \text{if} \quad S(z)<0. \tag{25}$$

The domain of definition of the variable z is determined by the inequality:

$$DT(z)\equiv\frac{J(z)^2}{[1+S(z)^2]^2}-\frac{J(z)^2-S(z)^2R_L^2}{1+S(z)^2}\geqslant 0 \tag{26}$$

where $DT(z)$ is the discriminant of (24).

4. Solutions and Ray Tracing in the Eye. In Fig. 6A the theoretical curve $e(x)$ is shown calculated with the parameters of eye 1 (Table 1) except that $R_t=295$ μm and $f=125$ μm. The solution at the periphery is not unique, there the function $e(x)$ bifurcates. In order to understand the peripheral bifurcation of the solution, consider Fig. 6B, which shows the (backward) ray tracing in the

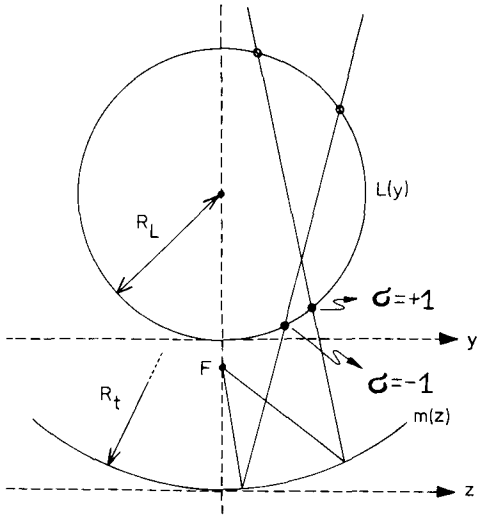

Figure 5. The diagram illustrates how the parameter σ in equation (24) is determined when both the rear surface of the lens and the *argentea* are spherical.

eye (the incident paraxial rays are omitted). Ray tracing is made using the series $[z_i, m(z_i)]$, $[y_i, L(y_i)]$ and calculating $[x_i, e(x_i)]$.

Starting from the focal point F, under special parameter configurations the rays of light reflected by the *argentea* and refracted by the rear surface of the lens converge such that they intersect, which is the reason of the peripheral bifurcation of the solution. Due to this bifurcation there are two different ways to construct an optical system without spherical aberration.

(i) A system with the theoretically calculated front surface between P_1 and P_3 (see Fig. 6A), the ray tracing of which is shown in Fig. 6C.

(ii) A system with the theoretically determined front surface between P_1, P_2 and P_4, P_3 (see Fig. 6A), the ray tracing of which is represented in Fig. 6D.

In case (i) the front surface of the lens is smooth. However, in case (ii) it has a discontinuity at P_2, P_4. Such a discontinuity would be disadvantageous in any biological systems with respect to its mechanical properties, and problematic regarding morphology and development. We shall touch upon this point briefly in the discussion. Therefore we reject this solution and consider further on only the solution (i). The branch P_3P_4 of the bifurcation (if it exists) is not considered.

5. The Shape of the Front Surface of the *Pecten* Lens as a Function of the Focal Length. The focal length f of the *Pecten* eye cannot be determined very accurately. The lens is soft, and must be handled carefully to prevent deformation. Land (1965) has measured the focal length in the intact eye as well

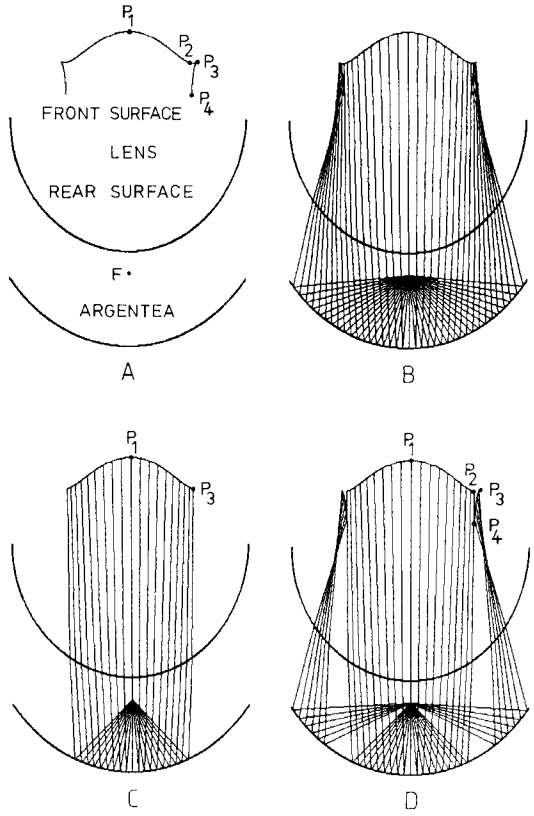

Figure 6. (A) Median section $e(x)$ of the theoretically calculated front surface of the *Pecten* lens with parameters of eye 1 (see Table 1) except that $R_1 = 295$ μm, $f = 125$ μm; F: focal point of the eye. The figure shows the bifurcation of the solution between P_3, P_2 and P_4. (B) As (A) with ray tracing in the eye. (C) One out of the two possible solutions for $e(x)$ between P_1 and P_3 with ray tracing. (D) The other possible solution between P_1 and P_2, and P_4 and P_3 with ray tracing. Here and in the subsequent figures we omitted the paraxial incident rays.

as that of the isolated lens. The focal length of the isolated lenses turned out to be about 45% larger on average than that measured *in situ*. In the opinion of Land the reason for this discrepancy was on the one hand that the lens had no single focal point, but there is a complex pattern with an extended region of focus. Another reason for the discrepancy might have been the erroneous assumption, that in the intact eye the optical and geometrical centres of the lens coincide.

Focal length f of the eye (Fig. 3) determines the image position. The image produced by refraction on the lens and reflexion at the *argentea* has to be formed on the distal retina. The optimal focal length f of a *Pecten* eye has been determined theoretically as follows. Varying f, we have sought for that

theoretical front profile, the shape of which fits best (least squares) the real front surface of the *Pecten* lens described and approximated by the fourth-degree equation (23). We made this analysis for both eye 1 and 2, the parameter configurations of which can be found in Table 1.

The results are shown in Figs 7 and 8 for eye 1 and 2, respectively, for three values of f. The shape of the theoretical front surface of the lens depends strongly on the focal length. In Figs 7 and 8 the ray tracing in the eye, the real front face of the lens described by (23) (thick curve), and the theoretical front surface of the lens (thin curve) are depicted. The ray tracing, of course, corresponds to the theoretically determined front surface. The two vertical thick lines starting from the front face of the lens represent the iris of the eye:

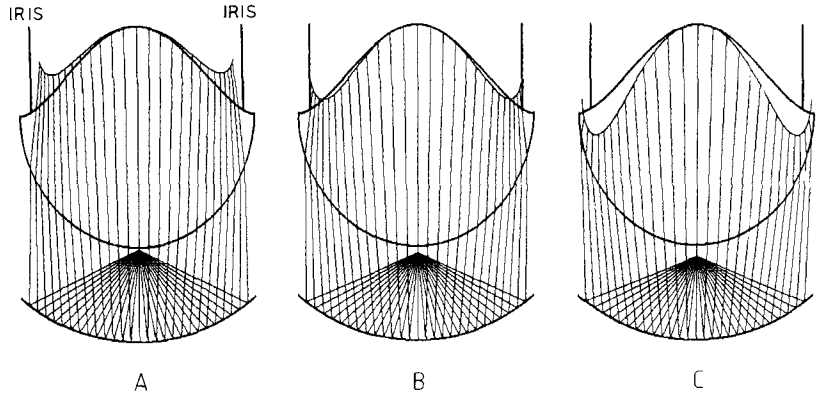

Figure 7. Median section of the eye showing the theoretically calculated front surface (thin curve) and the real one (thick curve) of the *Pecten* lens and ray tracing with parameters of eye 1 (Table 1) for $f=160$ μm (A), $f=153$ μm (B), $f=145$ μm (C).

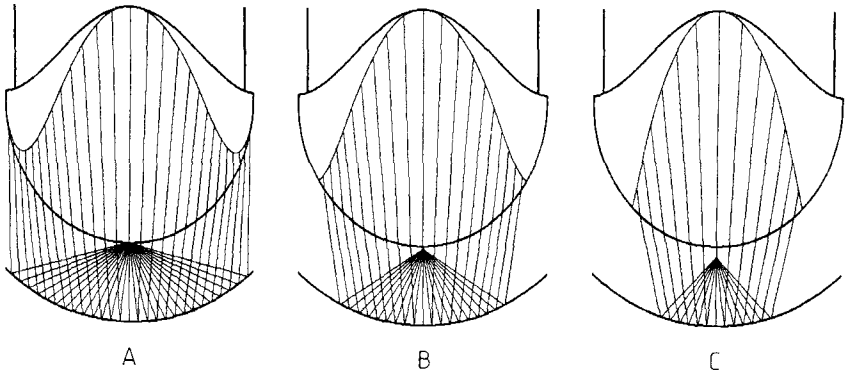

Figure 8. As Fig. 7 with parameters of eye 2 (Table 1) for $f=140$ μm (A), $f=135$ μm (B), $f=120$ μm (C).

paraxial rays of light can be received by the eye only within the area bounded by the iris.

In Fig. 7A and C the theoretical front surface lies above and below the real one, respectively. The theoretical front profile in Fig. 7B is the best fit to the real one. The optimal value of the focal length of eye 1 is therefore $f = 153$ μm. In case of eye 2 (Fig. 8) all the theoretical front surfaces lie below the real one; the difference between the theoretical and real profiles increases with decreasing f, and is the smallest when f has its maximal possible value $f_{max} = b$. However, the difference is still too large in this case.

The exact profile of the front face of the lens and the geometrical parameters of the eye of *Pecten* are very variable (Land, 1965). However, the theoretical shape of the front surface of the lens depends strongly on these parameters, as it can already be seen in Figs 7 and 8. We shall deal with this question in the following sections. We choose the parameter configuration of eye 1 for which with $f_{opt} = 153$ μm a relatively well fitting theoretical front profile has been found (Fig. 7B).

6. Dependence of the Theoretical Shape of the Front Face of the Lens on the Refractive Indices of the Eye. According to Land (1965) the refractive index of the *Pecten* lens is uniform ($n_L = 1.42$). The dependence of the theoretical shape of the front surface on the refractive index n_L of the homogeneous lens is shown in Fig. 9, obtained with the parameters of eye 1 for two values of the focal length f.

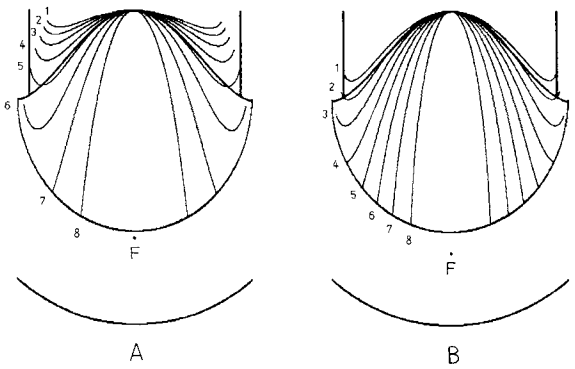

Figure 9. In this and the subsequent figures we illustrate how the variation of different parameters of eye 1 influences the front surface of the lens. Curves are derived for the optimal focal length $f = 153$ μm (A), and for a shorter suboptimal one of $f = 125$ μm (B). Here we varied the refractive index n_L of the lens within the range of 1.5 (curve 1) to 1.36 (curve 8) in steps of $\Delta n_L = 0.02$.

Observations made by Land (1965) on the isolated retina of the *Pecten* eye and on individual cells indicate that only the outer segments of the retina have a refractive index substantially higher than sea water. In the opinion of Land (1965) the effect of such a layer, less than 40 μm thick, on the focal length or on the position of the reflected image can be neglected and the retina can be considered optically homogeneous. In Fig. 10 the dependence of the theoretical shape of the front profile of the lens on the homogeneous refractive index n_r of the retina is shown, obtained again with the parameters of eye 1 for two different focal length f.

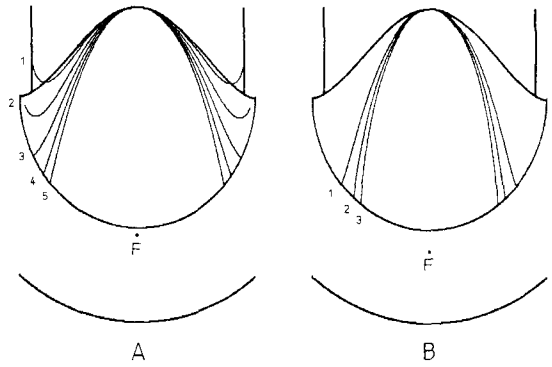

Figure 10. (A) The refractive index n_r of the retina varies from 1.34 (curve 1) to 1.50 (curve 5) in steps of $\Delta n_r = 0.04$. (B) $n_{r1} = 1.34$, $n_{r2} = 1.42$, $n_{r3} = 1.50$.

It can be seen in Figs 9 and 10 that the shape of the theoretical front face depends strongly on the optical parameters n_L and n_r of the eye.

7. Dependence of the Theoretical Shape of the Front Face of the Lens on the Geometrical Parameters of the Eye. In contrast to the refractive indices n_L and n_r of the lens and retina, the geometrical parameters of the *Pecten* eye are very variable (Land, 1965), therefore it is worth while to investigate the effect of their numerical values on the shape of the theoretical front profile of the lens.

The dependence of the theoretical shape of the front surface of the lens on the axial thickness a of the lens, the axial distance b between the rear face of the lens and the *argentea*, the radius of curvature R_L of the rear face of the lens and the radius of curvature R_t of the *argentea* are illustrated in Figs 11–14, respectively, for two different values of the focal length f.

8. Discussion. Our main objective was to find out to what extent the highly specialized front surface of the lens in the eye of *Pectens* corrects for the spherical aberration of the *argentea*. For this we assumed that in an ideally corrected eye all paraxially incident rays intersect in a true focal point on the

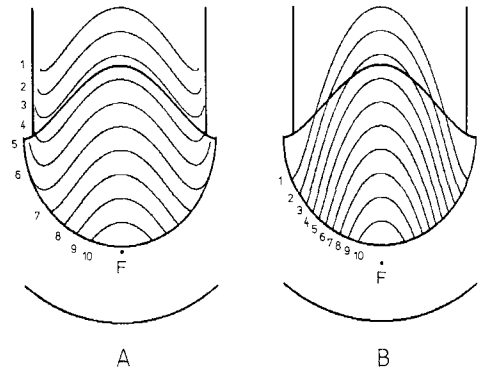

Figure 11. The axial thickness a of the lens varies from 500 μm (curve 1) to 50 μm (curve 10) in steps of $\Delta a = 50$ μm.

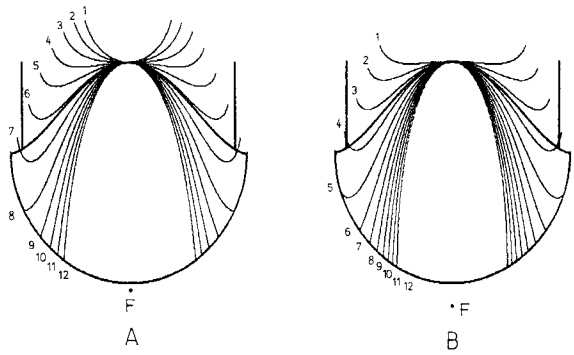

Figure 12. The axial distance b between the rear surface of the lens and the *argentea* varies from 220 μm (curve 1) to 110 μm (curve 12) in steps of $\Delta b = 10$ μm. (A) $\Delta f = 12$ μm, (B) $\Delta f = 40$ μm, where Δf is the axial distance between the focal point F and the rear surface of the lens. (The illustration of the varying position of the *argentea* is omitted.)

optical axis of the eye. We backtraced the rays from this point and calculated the corresponding front surface of the lens for different focal distances f. Our question was whether and at which focal distance the real front surface of the lens matches the calculated curves.

First we found that the equations have two different solutions, and, therefore, there are two possible surfaces which optimally correct for spherical aberration (Fig. 6C,D). One of them (Fig. 6D) appears to be disadvantageous, since it has a discontinuity in the periphery, and the rays impinging laterally to this discontinuity form an inverted image. Such a discontinuity would reduce the mechanical stability of the soft jelly-like lens and its light-collecting

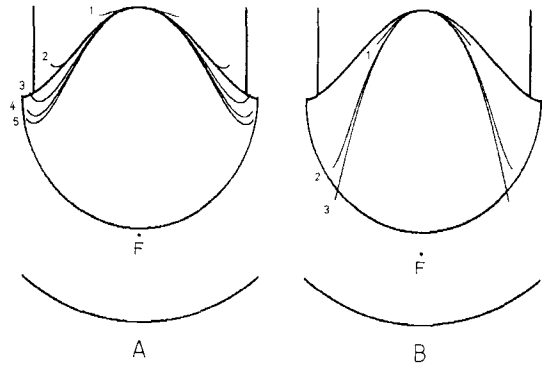

Figure 13. (A) The radius of curvature R_L of the lens varies from 100 μm (curve 1) to 500 μm (curve 5) in steps of $\Delta R_L = 100$ μm; (B) The radii of curvature $R_{L1} = 100$ μm, $R_{L2} = 200$ μm, and $R_{L3} = 300$ μm, correspond to the curves 1, 2 and 3, respectively. (The varying rear surface of the lens is not illustrated by a corresponding set of curves.)

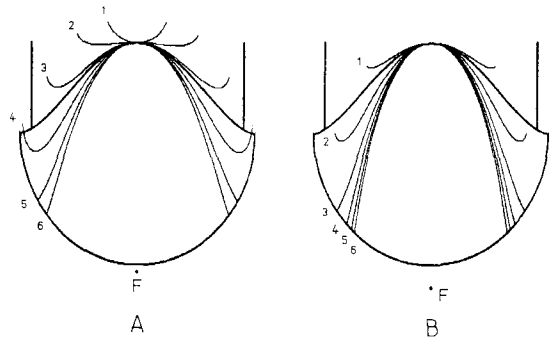

Figure 14. The radius of curvature R_t of the *argentea* varies from 290 (curve 1) to 490 μm (curve 6) in steps of $\Delta R_t = 40$ μm. (The illustration of the varying shape of the *argentea* is omitted.)

efficiency. It is unlikely that evolution brought about such a design. Therefore, we considered only the theoretical eye without discontinuity of the front surface.

Two different sets of experimentally obtained eye parameters were available to answer our question (Table 1), including distances (cf. Fig. 3) and refractive indices. We refer to the corresponding eyes as eye 1 and eye 2. For eye 1 with a focal length of $f = 153$ μm the theoretical curve fits well the real shape of the front surface of the lens (Fig. 7B), especially in the central region. However, even small deviations of the focal length from the optimal value leads to considerable deviations between the theoretical and the real surfaces (Fig. 7A,C).

With the parameters of eye 2 no agreement between theory and reality can be achieved within the entire realistic range of the focal distance f (Fig. 8). We confined, therefore, our further considerations to eye 1. We investigated how sensitive the front surface is to parameter variations at the optimal and at a slightly smaller suboptimal focal length f, in order to elucidate whether a set of parameters other than those observed might improve the *Pecten* eye.

The influence of the refractive index n_L *of the lens.* At the optimal focal length (Fig. 9A) the best fit is, of course, achieved with the measured value of n_L (curve labelled 5). Our question was whether, with another pair of the parameters f and n_L, a better match is possible. Indeed, the curve labelled 2 in Fig. 9B fits slightly better the real front surface than curve 5 in Fig. 9A. The price for this small improvement would be a considerable increase of the refractive index n_L to about 1.5, which could be realized only by a lens consisting of hard protein instead of a soft jelly-like substance.

The refractive index n_r *of the retina.* Except for a very thin layer the refractive index n_r of the retina is the same as that of sea water. An improvement of the optical properties of the eye could, therefore, be achieved only by a combination of increased value of n_r and a corresponding focal length. As demonstrated in Fig. 10, any increase of n_r leads to an increasing mismatch between the theoretical and the real surface, no matter whether the focal length f is optimal or suboptimal.

The axial thickness a *of the lens.* The shape of the front surface changes little with the axial thickness a at the optimal focal length f (Fig. 11A). However, at small values of a the aperture is considerably reduced. At a value of a higher than that obtained experimentally the scallop needed more material to build the lens, which might be a disadvantage. At a suboptimal focal length, no proper match is possible at any value of a (Fig. 11B).

The axial distance b *between the rear surface of the lens and the* argentea. The change of b drastically influences the profile of the front surface; the concave curves become convex when this parameter is increased (Fig. 12A). However, it also appears that for a shorter focal length there is a distance b such that the fit between the theoretical and real front surface is satisfactory (cf. curve 4 in Fig. 12B with $b = 190$ μm instead of 115 μm). Thus, the change of b can be compensated for by a corresponding change of f.

The radius of curvature R_L *of the lens.* A deviation from the measured value leads to increasing discrepancies between the real and the theoretical surfaces (Fig. 13A). A change of the focal length (with unchanged other parameters) cannot be compensated for by a change of the radius of curvature (Fig. 13B).

The radius of curvature R_t *of the* argentea. We obtain similar results to the former case (Fig. 14).

Interestingly, the peculiar design of the *Pecten* eye inspired Greguss (1985, 1986) to construct a photographic lens with a wide annular panoramic view.

In this work we have limited our analysis to consider only paraxial rays, and studied the degree of correction for spherical aberration only. Non-paraxial rays result in, of course, other types of optical aberrations: coma (Born and Wolf, 1964), astigmatism, distortion and curvature of field. (These are called primary wave aberrations.) However, the minimization or full correction for spherical aberration calls forth the decrease of other optical aberrations belonging to off-axis rays. Our main conclusion is that the degree of correction for spherical aberration in the *Pecten* eye is not as good as it could be. Scallop's eyes have certain correction, but not as fully as in the highly optimized eyes of some extinct trilobites (Clarkson and Levi-Setti, 1975; Horváth, 1989b; Horváth and Clarkson, 1992) or the water bug *Notonecta* (Schwind, 1980; Horváth, 1989a; Horváth and Greguss, 1989a,b).

The wide angular acceptance of the *Pecten* eye suggests that off-axis rays must contribute to a substantial portion of the image. The number of ommatidia in a common schizochroal trilobite eye was several hundred (Clarkson and Levi-Setti, 1975), in the *Notonecta* eye it is about 3700 (Schwind, 1980), however, scallops have a maximum of one hundred pallial eyes, and the visual field of each eye extends to 90–110° (Land, 1965). So in the case of full correction for spherical aberration in the *Pecten* eye the other four optical aberrations belonging to non-paraxial rays would anyway reduce the quality of image, at least peripherally. Therefore, there is no reason for using peripherally in the distal retina as large a density of photoreceptors as centrally. This may be the biooptical reason for the fact that the density of cells in the distal retina decreases towards the periphery (Land, 1965, 1968).

The relatively small degree of correction for spherical aberration of the *Pecten* eye goes necessarily together with the peripherally large degree of optical aberrations belonging to off-axis rays due to the large aperture of the eye. The biooptical reason for the difference between the degrees of correction for spherical aberration in the eyes of trilobites, backswimmers and scallops may be the following.

Trilobites with schizochroal and backswimmers with apposition compound eyes had/have to mate, capture prey and escape from predators in dim light, that is, they had/have a very complex repertory of behaviour in obscure environments. Therefore they developed a highly optimized visual system that forms high quality images, has a large light-collecting efficiency, and transfer of contrast.

On the contrary, scallops may not need such highly optimized eyes for perception of shadowing and movements in their optical environment. A

scallop with fully corrected eyes probably does not have an advantage over another one with eyes of a lower degree of correction for optical aberrations when considering their movement and shadow perception at least.

9. Conclusions. With proper parameters such as that of eye 1, the peculiar shape of the front surface of the lens in the *Pecten* eye compensates well for the spherical aberration caused by the spherical *argentea*. Small deviations of the parameters from suitable values causes substantial deviations from the optimality. Experimental investigations reveal great variability of the eye parameters (Land, 1965) (however, these variations might be the consequence of the technical difficulties while trying to measure the parameters of the eye). The degree of correction of the *Pecten* lens for spherical aberration might not be as good as it could be, and it necessarily goes together with the peripherally large degree of optical aberrations belonging to off-axis rays because of the large aperture of the eye. It seems reasonable to assume that the actual shape of the correcting surface of the lens may result from a compromise that would optimize the lens function over a wide cone of acceptance. Moreover, scallops might not necessarily need a very sharp image of their optical surroundings in the same way some extinct trilobites with schizochroal eyes needed to, or as the water bug, *Notonecta glauca*, needs. In addition, inadequacies of a single eye in *Pecten* might be compensated for with respect to visually guided behaviour by interaction with other eyes.

Thanks are due to Professor Pál Greguss, whose interest in the *Pecten* eye facilitated our motivation for this study. Financial support came from the Deutsche Forschungsgemeinschaft (SFB 307).

LITERATURE

Born, M. and E. Wolf. 1964. *Principles of Optics*, pp. 245–250 and pp. 212–217. Oxford: Pergamon Press.

Clarkson, E. N. K. and R. Levi-Setti. 1975. *Nature* **254**, 663–667.

Dakin, W. J. 1910. *Q. J. Micr. Sci.* **55**, 49–112.

Denton, E. J. 1970. *Phil. Trans. R. Soc. London* **B258**, 285–313.

Denton, E. J. 1971. *Sci. Am.* **224**, 65–72.

Greguss, P. 1985. *Opt. Laser Technol.* **17**, 41–45.

Greguss, P. 1986. *Panoramic Holocamera for Tube and Borehole Inspection.* International Seminar on Laser and Optoelectronic Technology in Industry—A State of the Art Review, 25–27 June 1986, Xiamen, P.R.C.

Hartline, H. K. 1938. *J. Cell. Comp. Physiol.* **11,** 465–477.

Horváth, G. 1989a. *J. theor. Biol.* **139**, 389–404.

Horváth, G. 1989b. *Math. Biosci.* **96**, 79–94.

Horváth, G. and E. N. K. Clarkson. 1992. Theoretical reconstruction of the change of form of the lens in the post-ecdysial development of the schizochroal eye of the Devonian trilobite *Phacops rana milleri* (Stewart 1927). *J. theor. Biol.*, in press.

Horváth, G. and P. Greguss. 1989a. *Appl. Optics* **28**, 1974–1976.
Horváth, G. and P. Greguss. 1989b. *Int. Agrophys.* **5**, 231–246.
Kennedy, D. 1963. *Sci. Am.* **209**, 122–130.
Land, M. F. 1965. *J. Physiol.* **179**, 138–153.
Land, M. F. 1966a. *J. exp. Biol.* **45**, 83–99.
Land, M. F. 1966b. *J. exp. Biol.* **45**, 433–447.
Land, M. F. 1968. *Symp. zool. Soc. London* **23**, 75–96.
Patten, W. 1886. *Pubbl. zool. Staz. Napoli* **6**, 542–756.
Schwind, R. 1980. *J. Comp. Physiol.* **140**, 59–68.
von Buddenbrock, W. and I. Moller-Racke. 1953. *Pubbl. zool. Staz. Napoli* **24**, 217–245.

Received 26 February 1991
Revised 17 November 1991